Regularization of covariant calculations of meson decay amplitudes at one-loop order: Properties of the $a_0(980)$ resonance

L. S. Celenza, Bo Huang, Huangsheng Wang, and C. M. Shakin*
Department of Physics and Center for Nuclear Theory, Brooklyn College of the City University of New York, Brooklyn, New York 11210
(Received 14 June 1999; published 22 November 1999)

The unitary quark model of Törnqvist and Roos provides an extremely interesting description of the properties of the scalar meson nonet. The model is quite phenomenological and has six parameters. In this work we are interested in seeing whether a theoretical foundation for the unitary quark model can be created using our generalized Nambu–Jona-Lasinio (NJL) model, which includes a covariant model of confinement. To make contact with Törnqvist's work, it is necessary to go beyond the leading vacuum polarization diagram of the NJL model, $J(P^2)$, which is of order n_c, and calculate the (complex) function $K(P^2)$, which is of order 1, and which describes the decay of $q\bar{q}$ states to the continuum of two-meson states. The central issue is the creation of a model for the regularization of the one-loop amplitudes with three vertices. We choose a regulator that has been used in our recent study of f_0 mesons. The same regularization is used for the $\pi\eta$, $K\bar{K}$, and $\pi\eta'$ channels, when studying the properties of the $a_0(980)$ resonance. The coupling to the decay channels described by $K(P^2)$ is an important feature of the model, since the mass of the a_0 mass would be 1090 MeV in the absence of such coupling. The peak width obtained for the $a_0(980)$ resonance is 23 MeV, which is smaller than the values of 50–100 MeV usually quoted. (Larger values may be obtained in our calculation with another form of the regulator.) While our model is not parameter free, we believe we have made significant progress toward putting the unitary quark model on a firmer foundation. [S0556-2813(99)04412-X]

PACS number(s): 13.25.−k, 12.39.Fe, 14.40.−n, 12.39.Ki

I. INTRODUCTION

In a series of papers we have been developing a generalized Nambu–Jona-Lasinio (NJL) model which includes a covariant model of confinement [1–11]. We have studied $\eta - \eta'$, $\phi - \omega$, and $\pi - a_1$ mixing, including both singlet-octet and pseudoscalar–axial-vector mixing, where appropriate [3]. We have also made a comprehensive fit to states of the pseudoscalar and vector meson nonets and have made some preliminary studies of the axial-vector and the scalar nonet of states. In these works, we have studied radial excitations up to 2 GeV [9] and beyond [11]. In addition, we have studied the spectrum of f_2 tensor mesons [10] and have calculated decay rates for the processes $\pi \to \gamma\gamma$, $\eta \to \gamma\gamma$, and $\eta' \to \gamma\gamma$ [7,8]. Reference [5] contains a study of the radial excitations of the pion and a calculation of the rates for the processes $\pi(1300) \to \pi\sigma$ and $\pi(1300) \to \pi\rho$.

In the present work we extend our calculations to consider the $a_0(980)$ resonance, with particular attention paid to the role of meson decay channels in modifying the properties of that meson. [The $a_0(980)$ resonance is a member of the scalar nonet, which is depicted in Fig. 1.] Our work is closely related to that of Törnqvist who studied the scalar nonet of states in a unitary quark model which required the introduction of six parameters [12]. In that work, the meson-decay amplitudes for the channels $K\pi$, $K\eta$, $K\eta'$, $\pi\pi$, $\pi\eta$, $\pi\eta'$, $\eta\eta$, $\eta\eta'$, and $\eta'\eta'$ were parametrized and used to construct the imaginary parts of the various vacuum polarization functions, $\Pi(P^2)$. The real part of each $\Pi(P^2)$ was then obtained *via* a dispersion relation. In addition, a ''bare mass,'' m_0, was assigned to the $q\bar{q}$ states, so that the inverse meson propagator had the form $P^2 - m_0^2 + \Pi(P^2)$. (A value of $m_0 = 1420$ MeV was used, if the $q\bar{q}$ system was composed of only u and d quarks. This ''bare mass'' finds a natural interpretation in our analysis of the unitary quark model.) Törnqvist was able to fit a large body of data using his phenomenological model [12]. In the work reported upon here, we will see that our generalized NJL model can provide a theoretical foundation for the unitary quark model. In principle, no new parameters, other than those determined in our earlier studies [1–11], should be required. However, we require a procedure for regularizing one-loop amplitudes with three vertices that describe meson decay. We use a Gaussian regulator for these amplitudes, that has been used in a recent study of f_0 mesons [13]. (The results are quite sensitive to the parameter choice made for the regulator. That is in contrast to the situation found when fitting meson spectra, where a change in the regularization parameter may be compensated for by a change in the magnitude of the coupling con-

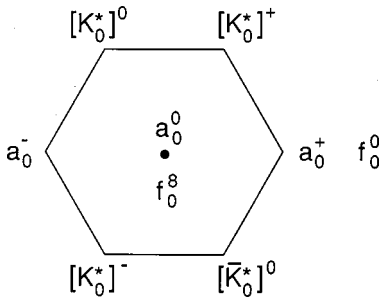

FIG. 1. States of the scalar nonet are shown.

*Electronic address: casbc@cunyvm.cuny.edu

stants of the short-range NJL interaction. For example, we have made use of Minkowski momentum-space cutoffs of $|\mathbf{k}| \leqslant \Lambda_3$ with $\Lambda_3 = 0.622$ GeV [9] and $\Lambda_3 = 0.80$ GeV [11], with similar results for meson spectra. A Gaussian regulator has also been used in Ref. [13].)

The organization of our work is as follows. In Sec. II we describe some aspects of the vacuum polarization diagrams of the NJL model and discuss their role in the calculation of various T matrices. In Sec. III we describe the calculation of decay amplitudes for the decay of scalar-isovector mesons to the two-meson continuum states. In Sec. IV we present our numerical results for various vacuum polarization functions and T matrices. Section V is devoted to some further discussion and conclusions.

II. VACUUM POLARIZATION DIAGRAMS OF A GENERALIZED NJL MODEL

Since our methods of calculation have been described elsewhere [1–11,13], we will only provide a short review of our formalism. The Lagrangian of the model is

$$\mathcal{L} = \bar{q}(i\not{\partial} - m^0)q + \frac{G_S}{2}\sum_{i=0}^{8}[(\bar{q}\lambda^i q)^2 + (\bar{q}i\gamma_5\lambda^i q)^2] - \frac{G_V}{4}\sum_{i=0}^{8}[(\bar{q}\gamma^\mu\lambda^i q)^2 + (\bar{q}\gamma^\mu\gamma_5\lambda^i q)^2] + \frac{G_D}{2}\{\det[\bar{q}(1+\gamma_5)q] + \det[\bar{q}(1-\gamma_5)q]\} + \mathcal{L}_{\rm conf}, \tag{2.1}$$

while $\mathcal{L}_{\rm conf}$ denotes our model of confinement. In Eq. (2.1), m^0 is the current quark mass matrix, $m^0 = \mathrm{diag}(m_u^0, m_d^0, m_s^0)$, the λ_i $(i = 1, \ldots, 8)$ are the Gell-Mann matrices, and $\lambda_0 = \sqrt{2/3}I$, with I being the unit matrix in flavor space. The fourth term is the 't Hooft interaction. (We note that additional interaction terms are needed for the study of tensor mesons [10].)

We first introduce the vacuum polarization function required for the study of scalar-isovector excitations of the NJL model, in the absence of a model of confinement

$$-iJ_S(P^2) = (-1)2n_c \times \int \frac{d^4k}{(2\pi)^4}\mathrm{Tr}[iS(P/2+k)iS(-P/2+k)]. \tag{2.2}$$

[See Fig. 2(a).] Here $n_c = 3$ and the factor 2 arises from the flavor trace. The propagator is $S(P) = (\not{P} - m + i\epsilon)^{-1}$, where m is the constituent quark mass. The function defined in Eq. (2.2) becomes complex for $P^2 > (2m)^2$, since both the quark and antiquark can go on their (positive) mass shell. This unphysical feature limits the use of the NJL model to relatively low energies. To remedy this defect, we introduce a confining interaction V^C and a corresponding vertex operator $\bar{\Gamma}_S(P,k)$, shown as a filled triangle area in Fig. 2(b). In Figs.

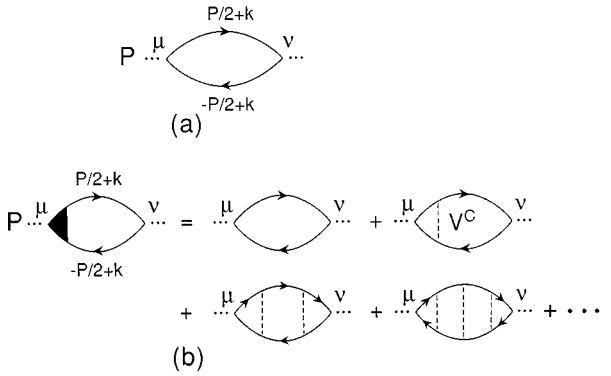

FIG. 2. (a) The diagram shows the basic vacuum polarization diagram of the NJL model in the absence of a confinement model. (b) The diagram serves to define the tensor $J^{\mu\nu}(P)$ in the presence of a confinement vertex, represented by the shaded triangular area (see Fig. 3). The right-hand side of the figure shows a perturbative expansion for $J^{\mu\nu}(P)$.

2(b) and 3(b), we show a perturbative expansion of the vertex. With the vertex in place, $J_S(P^2)$ is real and given by

$$-iJ_S(P) = (-1)2n_c\int\frac{d^4k}{(2\pi)^4}\mathrm{Tr}[iS(P/2+k) \times \bar{\Gamma}_S(P,k)iS(-P/2+k)]. \tag{2.3}$$

Equations for $\bar{\Gamma}_S(P,k)$ are given in Appendix A.

Values for $J_S(P^2)$, calculated in Ref. [9], are shown in Fig. 4. We note that $J_S(P^2)$ has singularities when the vertex operator is singular, which occurs at the energies of bound states in the confining field (in the absence of the NJL interaction). If we work in the rest frame of the scalar meson, it is useful to define the functions Γ_S^{+-}, Γ_S^{-+}, Γ_S^{++}, and Γ_S^{--}. We introduce

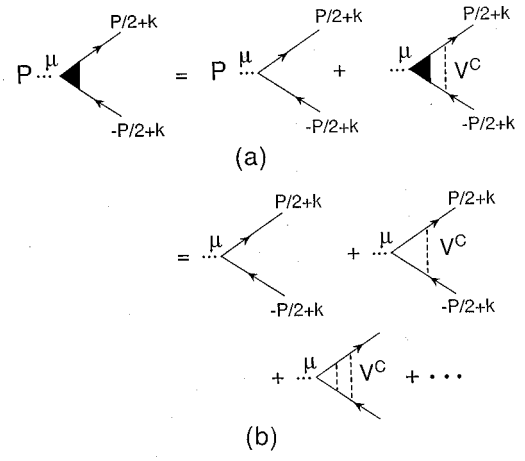

FIG. 3. (a) The equation for the vertex operator $\Gamma^\mu(P,k)$ is shown. The vertex is represented by the filled triangular area and the dashed line represents the confining interaction. (b) A perturbative expansion is shown for the equation in (a). We see that the vertex serves to sum a ''ladder'' of confining interactions.

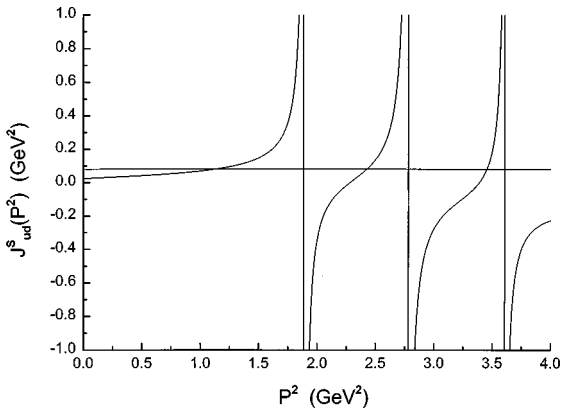

FIG. 4. The figure exhibits the values of the function $J^S_{ud}(P^2)$, when the subscripts are a reminder that the calculation is made for $m_u = m_d = 0.364$ GeV. The horizontal line represents G_{88}^{-1} and yields a graphical solution of the equation $G_{88}^{-1} - J_S(P^2) = 0$.

$$\Lambda^{(+)}(\mathbf{k}) = \frac{\not k + m}{2m} \tag{2.4}$$

and

$$\Lambda^{(-)}(-\mathbf{k}) = \frac{\not k + m}{2m}, \tag{2.5}$$

with $k^\mu = [E(\mathbf{k}), \mathbf{k}]$ and $\tilde{k}^\mu = [-E(\mathbf{k}), \mathbf{k}]$. We then define

$$\Lambda^{(+)}(\mathbf{k})\overline{\Gamma}_S(P,k)\Lambda^{(-)}(-\mathbf{k}) = \Gamma_S^{+-}(P,k)\Lambda^{(+)}(\mathbf{k})\Lambda^{(-)}(-\mathbf{k}), \tag{2.6}$$

$$\Lambda^{(+)}(\mathbf{k})\overline{\Gamma}_S(P,k)\Lambda^{(+)}(\mathbf{k}) = \Gamma_S^{++}(P,k)\Lambda^{(+)}(\mathbf{k})\Lambda^{(+)}(\mathbf{k}), \tag{2.7}$$

etc. It is found that $\Gamma_S^{+-}(P,k) = \Gamma_S^{-+}(P,k)$ and $\Gamma_S^{++}(P,k) = \Gamma_S^{--}(P,k)$. It is readily seen that $J_S(P^2)$ depends only upon $\Gamma_S^{+-}(P^2)$, the propagators appearing in Eq. (2.3), and the regularization scheme adopted. Note that, since $\Gamma_S^{+-}(P,k)$ vanishes when *both* the quark and antiquark in Eq. (2.3) go on mass shell, $J_S(P^2)$ is a real function, without spurious cuts in the complex P^2 plane. While $J_S(P^2)$ is of order n_c, the next important term, $K_S(P^2)$, which is shown in Fig. 5(b), is of order 1. [The function $\Pi(P^2)$ of Törnqvist's work is related to our function $K_S(P^2)$.] We have $\Pi(P^2) = -g^2(P^2)K_S(P^2)$, where $g(P^2)$ is the meson-quark coupling constant, which is momentum dependent, in general. Note that there is no function analogous to $J_S(P^2)$ in Törnqvist's work.

In this work we study the properties of the $a_0(980)$ resonance. There is some difficulty in extracting a width for the $a_0(980)$ resonance from the data. For example, in the compilation of experimental data by the Particle Data Group, we find a broad range of values, with a suggested peak width of 50–100 MeV, although widths as small as 30 MeV have been found in one experiment [15]. We note that Törnqvist obtains 100 MeV for the peak width [12].

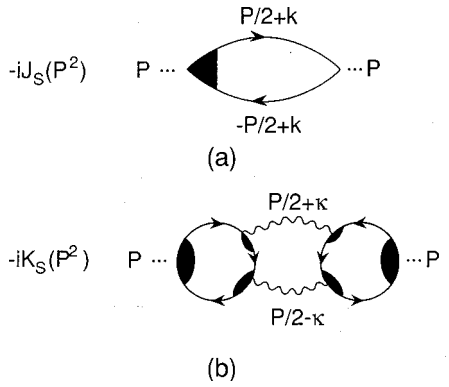

FIG. 5. (a) The vacuum polarization diagram that serves to define $-iJ_S(P^2)$ is shown. The shaded triangular region represents the (scalar) confining vertex $\overline{\Gamma}_S(P,k)$. (b) The vacuum polarization diagram that serves to define $-iK_S(P^2)$ is shown. The wavy lines denote mesons, while the shaded region represents the confinement vertices $\overline{\Gamma}_S(P,k)$ or $\overline{\Gamma}_P(P,k)$. (The only singularities of this diagram arise when the mesons go on mass shell.)

At this point, we describe the role played by the functions, $J_S(P^2)$ and $K_S(P^2)$, in parametrizing the T matrix in a simple case, with a single open channel. We consider the T matrix

$$t_S(P^2) = -\frac{G_S}{1 - G_S[J_S(P^2) + K_S(P^2)]}, \tag{2.8}$$

which we may write as

$$t_S(P^2) = -\frac{1}{G_S^{-1} - [J_S(P^2) + \mathrm{Re}\,K_S(P^2)] - i\,\mathrm{Im}\,K_S(P^2)}. \tag{2.9}$$

We expand $J_S(P^2) + \mathrm{Re}\,K_S(P^2)$ about the mass m_R that satisfies the equation

$$G_S^{-1} - [J_S(m_R^2) + \mathrm{Re}\,K_S(m_R^2)] = 0, \tag{2.10}$$

so that

$$t_S(P^2) \simeq \frac{1}{(P^2 - m_R^2)\left[\dfrac{\partial J_S(P^2)}{\partial P^2} + \dfrac{\partial\,\mathrm{Re}\,K_S(P^2)}{\partial P^2}\right] + i\,\mathrm{Im}\,K_S(m_R^2)}. \tag{2.11}$$

Here the derivatives are evaluated at $P^2 = m_R^2$. We then define

$$g^{-2} = \left.\frac{\partial J_S(P^2)}{\partial P^2}\right|_{P^2 = m_R^2}, \tag{2.12}$$

$$Z = \left[1 + g^2 \left.\frac{\partial\,\mathrm{Re}\,K_S(P^2)}{\partial P^2}\right|_{P^2 = m_R^2}\right]^{-1}, \tag{2.13}$$

and $\tilde{g}=Z^{1/2}g$ so that

$$t_S(P^2)=\frac{\tilde{g}^2}{P^2-m_R^2+im_R\Gamma_R}, \tag{2.14}$$

with $m_R\Gamma_R=\tilde{g}^2\,\mathrm{Im}\,K_S(m_R^2)$. The function $t_S(P^2)$ has an obvious physical interpretation.

Now let us consider the multichannel case, with N channels. It is then useful to define a dimensionless T matrix for channel 1 to be

$$T_{11}(P^2)=-\frac{\mathrm{Im}\,K_1(P^2)}{G_S^{-1}-[J_S(P^2)+\mathrm{Re}\,K_T(P^2)]-i\,\mathrm{Im}\,K_T(P^2)}, \tag{2.15}$$

where $K_T(P^2)=\Sigma_{i=1}^{N}K_i(P^2)$. (If only a single channel is open, we may write $T(P^2)=-\exp[i\delta]\sin\delta$, where δ is the phase shift.) In this work, the channels considered are $\pi\eta$, $K\bar{K}$, and $\pi\eta'$, where the $\pi\eta$ is channel 1, $K\bar{K}$ is channel 2, and $\pi\eta'$ is channel 3. Therefore, $T_{11}(P^2)$ describes $\pi-\eta$ scattering [12] with inelasticity arising at the thresholds for the $K\bar{K}$ and $\pi\eta'$ channels.

We now describe the procedure used to calculate $\mathrm{Re}\,K_i(P^2)$ for each channel. The first observation is that, when $G_S=G_D=0$, the confining potential has bound P states at $P^0=1.373$, 1.665, 1.898, 2.098, 2.263, and 2.410 GeV. The confining vertex is singular at each of these energies, giving rise to singularities in $J_S(P^2)$ and $K_i(P^2)$ [See Fig. 4]. However, it can be seen that double counting of diagrams arises if these singularities were to appear in $K_i(P^2)$. For the case $\mathbf{P}=0$, the singularities in $K_i(P^2)$ may be removed by the following procedure. We define a ''wave function''

$$\Psi^{+-}(P^0,|\mathbf{k}|)=\frac{\Gamma_S^{+-}(P^0,|\mathbf{k}|)}{P^0-2E(\mathbf{k})}, \tag{2.16}$$

and then systematically orthogonalize $\Psi^{+-}(P^0,|\mathbf{k}|)$ to the bound-state wave functions in the confining field [13]. The result of this procedure yields a ''wave function'' $\Phi^{+-}(P^0,|\mathbf{k}|)$ and a vertex $\hat{\Gamma}_S^{+-}(P^0,|\mathbf{k}|)=[P^0-2E(\mathbf{k})]\Phi^{+-}(P^0,|\mathbf{k}|)$ that are free of the singularities described above.

Using the vertex $\hat{\Gamma}_S^{+-}(P^0,|\mathbf{k}|)$, we can calculate $\mathrm{Im}\,K_i(P^2)$. We then obtain the values of $\mathrm{Re}\,K_i(P^2)$ using the dispersion relation

$$\mathrm{Re}\,K_i(P^2)=-\frac{P}{\pi}\int dP'^2\frac{\mathrm{Im}\,K_i(P'^2)}{P^2-P'^2}. \tag{2.17}$$

We place an upper limit of 6.0 GeV^2 on the integral in Eq. (2.17).

We have noted that the integrals that yield $J_S(P^2)$ require regularization. If we calculate $J_S(P^2)$ in the frame where $\mathbf{P}=0$, we may insert a Gaussian regulator of the form $R(\mathbf{k}^2)=\exp[-\mathbf{k}^2/\alpha^2]$ in Eq. (2.2) or Eq. (2.3). That form

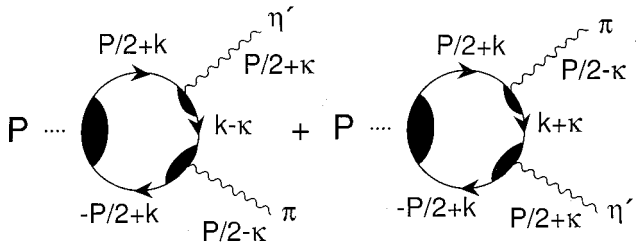

FIG. 6. The diagram that defines the amplitude $M(P^2)$ for the decay to the $\pi\eta'$ channel. The mesons are represented by wavy lines and are on mass shell. We designate the amplitude of (a) as the direct term and that of (b) as the exchange term.

may be written in a covariant fashion, so that it may be used in any frame. For example, with reference to Fig. 5, we may define

$$k_c^\mu=k^\mu-(k\cdot P)P^\mu/P^2 \tag{2.18}$$

and write

$$R(k_c^2)=\exp[k_c^2/\alpha^2]. \tag{2.19}$$

Note that $k_c^2=-\mathbf{k}^2$ in the frame in which $\mathbf{P}=0$. [In this work we use $\alpha=0.605$ GeV, when regulating $J_S(P^2)$.]

III. COVARIANT CALCULATION OF MESON DECAY AMPLITUDES

The decay amplitude calculated in this work is shown in Fig. 6 for the $\pi\eta'$ channel. The momentum entering the diagram is P, the η' has momentum $P/2+\kappa$, and the π has momentum $P/2-\kappa$, with both the η' and π on mass shell. The shaded areas represent our confining vertex functions, which we describe in further detail in Appendix B. It is useful to complete the integral over k^0, after writing each propagator using the representation

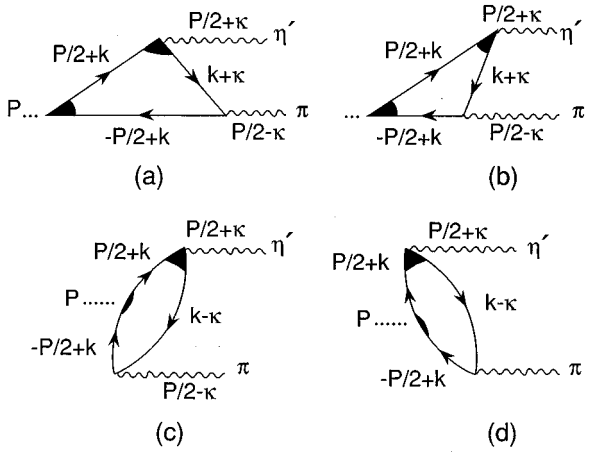

FIG. 7. Various diagrams that arise upon completing the integral over k^0 in the calculation of $M(P^2)$ shown in Fig. 6(a). There are two additional diagrams that serve to double the contribution of the diagrams in (c) and (d). The shaded regions denote the confinement vertices of the model. (We neglect confinement for the pion in our calculations.) Here, lines directed to the right represent quarks, while lines directed to the left represent antiquarks.

$$S(p)=\frac{m}{E(\mathbf{p})}\left[\frac{\Lambda^{(+)}(\mathbf{p})}{p^0-E(\mathbf{p})+i\epsilon}-\frac{\Lambda^{(-)}(-\mathbf{p})}{p^0+E(\mathbf{p})-i\epsilon}\right]. \tag{3.1}$$

The k^0 integral is completed in either the upper or lower k^0 plane. Since there are three propagators for each diagram, eight terms are obtained when using Eq. (3.1). However, only six of these are nonzero. Four of the six terms are shown in Fig. 7, where the shaded region denotes the confining vertex. [The other two nonzero terms serve to double the contribution of the amplitudes in Figs. 7(c) and 7(d).]

In order to better understand the role of confinement and covariance in our calculation, we present expressions for two of the diagrams in Fig. 7. For example, for Fig. 7(a), we have

$$M_1^{\eta\pi}(P^2)=M_1^{\eta\pi(1)}(P^2)+M_1^{\eta\pi(2)}(P^2), \tag{3.2}$$

with $\mathbf{P}=0$, $P^0=E_\pi(\boldsymbol{\kappa})+E_{\eta'}(\boldsymbol{\kappa})$, and

$$M_1^{\eta\pi(1)}(P^2)=n_c\int\frac{d^3k}{(2\pi)^3}\left[\frac{1}{E_\pi(\mathbf{k})-E(\mathbf{k})-E(\mathbf{k}-\boldsymbol{\kappa})}\right]\{2[m\mathbf{k}\cdot(\mathbf{k}-\boldsymbol{\kappa})-m\mathbf{k}^2]\}$$
$$\times\left(\frac{1}{2E^2(\mathbf{k})E(\mathbf{k}-\boldsymbol{\kappa})}\right)\frac{\hat\Gamma_S^{+-}(P^0,|\mathbf{k}|)}{P^0-2E(\mathbf{k})}g_{\pi qq}[h_1b_0(m_{\eta'}^2,k_{c,\eta'}^2)-m_{\eta'}^2h_2d_1(m_{\eta'}^2,k_{c,\eta'}^2)]R(k_{c,s}^2). \tag{3.3}$$

Here, h_1 and h_2 are constants defined in Appendix B. The functions $b_0(m_{\eta'}^2,k_{c,\eta'}^2)$ and $d_1(m_{\eta'}^2,k_{c,\eta'}^2)$ implement our confinement model and are also defined in Appendix B. The function $R(k_{c,s}^2)$ is a covariant Gaussian regulator

$$R(k_{c,s}^2)=\sqrt{\frac{2}{3}}\exp\left[\frac{k_{c,s}^2}{\alpha_1^2}\right], \tag{3.4}$$

where $\alpha_1=0.325\,\mathrm{GeV}$. (That value was also used in Ref. [13].) Here $k_{c,s}^2$ is the square of the four-vector defined in Eq. (2.18). [By choosing α_1 approximately, we can adjust the relative magnitude of $J_S(P^2)$ and $K_S(P^2)$. That is an important feature of our regularization scheme. For example, it is desirable that $|\mathrm{Re}\,K_S(P^2)|$ be less than about 25% of $J_S(P^2)$, a criterion that is consistent with $1/n_c$ counting procedures.]

Because of the small pion mass, the first bracketed term in Eq. (3.3) is not singular. Our confinement model is such that $\hat\Gamma^{+-}(P^0,|\mathbf{k}|)/[P^0-2E(\mathbf{k})]$ is finite. The function $M_1^{\eta'\pi(2)}(P^2)$, which has a similar expression to that given in Eq. (3.3), is not given here [see Appendix B]. We see that there are no singularities associated with the η' vertex of Fig. 7(a).

We now consider Fig. 7(b) and define

$$M_2^{\eta'\pi}(P^2)=M_2^{\eta'\pi(1)}(P^2)+M_2^{\eta'\pi(2)}(P^2), \tag{3.5}$$

with

$$M_2^{\eta'\pi(1)}(P^2)=-n_c\int\frac{d^3k}{(2\pi)^3}\left[\frac{1}{E(\mathbf{k})-E_{\eta'}(\boldsymbol{\kappa})+E(\mathbf{k}-\boldsymbol{\kappa})}\right]\{2[m\mathbf{k}\cdot(\mathbf{k}-\boldsymbol{\kappa})-m\mathbf{k}^2]\}$$
$$\times\left(\frac{1}{2E^2(\mathbf{k})E(\mathbf{k}-\boldsymbol{\kappa})}\right)\frac{\hat\Gamma_S^{+-}(P^0,|\mathbf{k}|)}{P^0-2E(\mathbf{k})}g_{\pi qq}[h_1b_0(m_{\eta'}^2,k_{c,\eta'}^2)-m_{\eta'}^2h_2d_1(m_{\eta'}^2,k_{c,\eta'}^2)]R(k_{c,s}^2). \tag{3.6}$$

There are two terms in Eq. (3.6) that would be singular in the absence of our confinement model. The first bracketed term in Eq. (3.6) has a zero value for the denominator, when the quark and the antiquark at the η' vertex go on mass shell. However, our confinement model is such that if we calculate all the terms describing decay to the $\pi\eta'$ channel, the numerator of the bracketed term has a corresponding zero at that point, leading to a finite value for the amplitude. As noted above, the term $\hat\Gamma^{+-}(P^0,|\mathbf{k}|)/[P^0-2E(\mathbf{k})]$ is also finite. We have seen that, if $\mathbf{P}=0$, the scalar vertex may be expressed in terms of $\hat\Gamma_S^{+-}(P^0,|\mathbf{k}|)$, when calculating the diagrams of Figs. 7(c) and 7(b). For the diagrams of Fig. 7(c) and 7(d), the scalar vertex introduces a factor of $\Gamma_S^{++}(P^0,|\mathbf{k}|)$. That function plays only a minor role in the calculation and little is changed if we put $\Gamma_S^{++}(P^0,|\mathbf{k}|)=\Gamma_S^{--}(P^0,|\mathbf{k}|)=1$. The treatment of the η' vertex in Fig. 7(c) is similar to that described for the η' vertex in Fig. 7(b). When we evaluate the diagram in Fig. 7(d) we do not encounter any singular terms, since $m_\pi<2m_u$, where m_u is the constituent mass of the up quark. (Here, $m_u=m_d=0.364\,\mathrm{GeV}$ and $m_s=0.565\,\mathrm{GeV}$.)

For a given channel, $\pi\eta$, $K\overline{K}$, or $\pi\eta'$, the summation of all relevant amplitudes defines a function $M_i(P^2)$. Then, for that channel,

$$\mathrm{Im}\,K_i(P^2)=\frac{S_i}{8\pi}\,\frac{\kappa_{\rm on}}{P^0}\,|M_i(P^2)|^2, \tag{3.7}$$

where, for the $\pi\eta'$ channel, for example,

$$\kappa_{\rm on}^2=\frac{[(P^0)^2-m_\pi^2-m_{\eta'}^2]^2-4m_\pi^2m_{\eta'}^2}{4(P^0)^2}. \tag{3.8}$$

In Eq. (3.7), S_i is a statistical factor arising, in part, from the flavor trace. For the $\pi\eta$ and $\pi\eta'$ channels, we take $S=1$, since the flavor trace is incorporated in the definition of h_1 and h_2. (See Appendix B.)

IV. RESULTS OF NUMERICAL CALCULATIONS

For the channels $\pi\eta$, $K\bar{K}$, and $\pi\eta'$ we have calculated $\mathrm{Im}\,K_i(P^2)$ and $\mathrm{Re}\,K_i(P^2)$ $(i=1,2,3)$ using the vertex functions given in Appendixes B and C. [The orthogonalization procedure that leads to replacing $\Gamma_S^{+-}(P^0,|\mathbf{k}|)$ by $\hat{\Gamma}_S^{+-}(P^0,|\mathbf{k}|)$ is also used.] For the η and η', we include the complete structure of the vertex that arises when calculating both singlet-octet and pseudoscalar–axial-vector mixing [8]. (We remark that it is essential to include a model of confinement for the η' when calculating the decay amplitude for the $\pi\eta'$ channel.) Here we have used the regulator of Eq. (3.4), with $\alpha_1=0.325$ GeV. Our results for $\mathrm{Im}\,K_i(P^2)$ and $\mathrm{Re}\,K_i(P^2)$ are given in Figs. 8–10. The values of $\mathrm{Re}\,K_i(P^2)$ are obtained from $\mathrm{Im}\,K_i(P^2)$ upon using Eq. (2.17).

For the calculation of $J_s(P^2)$ we use a Gaussian regulator of the form $\exp[-\mathbf{k}^2/\alpha^2]$ with $\alpha=0.605$ GeV. Our value for G_{88} is 12.46 GeV^{-2}. If we solve the equation $G_{88}^{-1}-J_s(P^2)=0$, we find the mass of the a_0 to be 1090 MeV. We may add $\mathrm{Re}\,K_T(P^2)$ to $J_s(P^2)$ and attempt to solve the equation $G_{88}^{-1}-J_s(P^2)-\mathrm{Re}\,K_T(P^2)=0$. However, the cusplike behavior seen in Figs. 8–10 makes that procedure problematic. Therefore, it is best to include $\mathrm{Im}\,K_T(P^2)$ at the same time that we introduce $\mathrm{Re}\,K_T(P^2)$.

We now consider the function

$$|T_{11}|^2=\frac{[\mathrm{Im}\,K_1(P^2)]^2}{\{G_S^{-1}-[J_S(P^2)+\mathrm{Re}\,K_T(P^2)]\}^2+[\mathrm{Im}\,K_T(P^2)]^2}. \tag{4.1}$$

(For an elastic resonance, $|T_{11}|^2$ is equal to $\sin^2\delta$, where δ is the phase shift.) When using Eq. (4.1), we found it necessary to add $\Delta K_T=0.008$ GeV^2 to $\mathrm{Re}\,K_T(P^2)$ to move the a_0 mass to 974 MeV (see Fig. 11). The parameter ΔK_T is the only parameter used in our analysis that has not been fixed in our earlier work. It is meant to represent contributions to $\mathrm{Re}\,K_T(P^2)$ from decay channels whose effects have not been calculated in this work or to compensate for a calculation of $\mathrm{Im}\,K_T(P^2)$ that yields a result that is too small. Our value for the peak width at half-maximum is 23 MeV, which may be seen in Fig. 11. The width of 23 MeV suggests that we have underestimated $\mathrm{Im}\,K_1(P^2)$. Therefore, we multiply $\mathrm{Im}\,K_1(P^2)$ by 2 and obtain the curve shown in Fig. 12, where $\Gamma_{\rm peak}=47$ MeV.

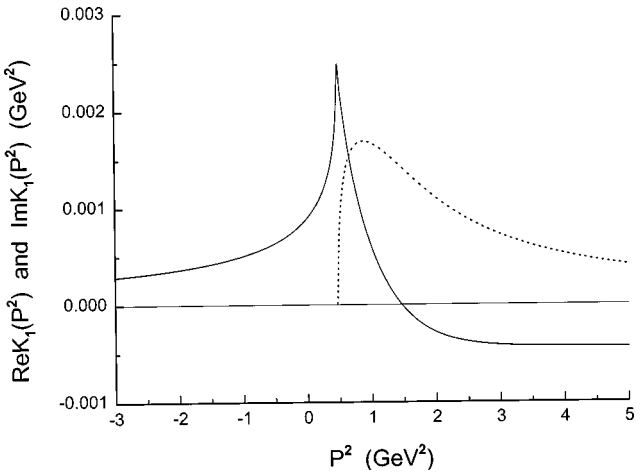

FIG. 8. The values of $\mathrm{Im}\,K_1(P^2)$ and $\mathrm{Re}\,K_1(P^2)$ are shown for the meson channel $\pi\eta$. [See Fig. 5(b).] Here $\alpha_1=0.325$ GeV.

V. DISCUSSION

In this work we have studied the regularization of loop integrals that describe meson decay in a generalized NJL model, which includes a covariant model of confinement, and made an application in a study of the $a_0(980)$ resonance. It was found that the choice of the covariant regulator of Eq. (3.4) gave reasonable results. We have also seen that our model can provide a theoretical basis for the unitary quark model of Törnqvist and Roos [12,16].

The study of the $a_0(980)$ resonance is made complicated by the $K\bar{K}$ channel, which has a 990 MeV threshold. In this regard, it is generally believed that the ''peak width'' of the $a_0(980)$ resonance can be distinguished from the total width when one studies the pole structure of the scattering amplitudes in the complex plane. For example, in Ref. [17], a K-matrix analysis leads to a mass and total width for the $a_0(980)$ resonance of $m=982\pm3$ MeV and $\Gamma=92\pm8$ MeV. However, the features responsible for the a_0 peak yield a full width at half maximum of 45 MeV, which is about half the

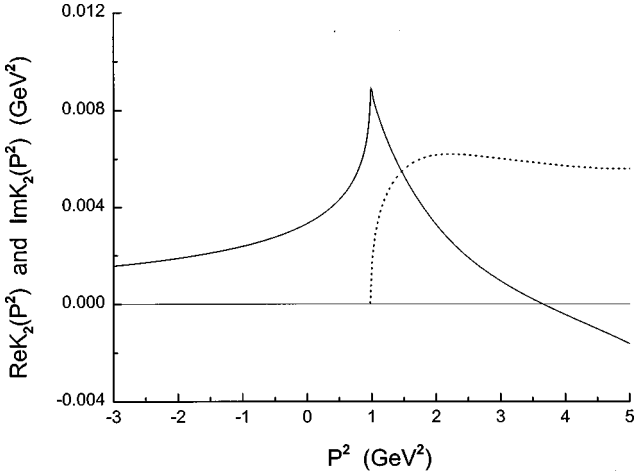

FIG. 9. The values of $\mathrm{Im}\,K_2(P^2)$ and $\mathrm{Re}\,K_2(P^2)$ are shown for the meson channel $K\bar{K}$. (This channel includes both $K^0\bar{K}^0$ and K^+K^- states.) Here $\alpha_1=0.325$ GeV.

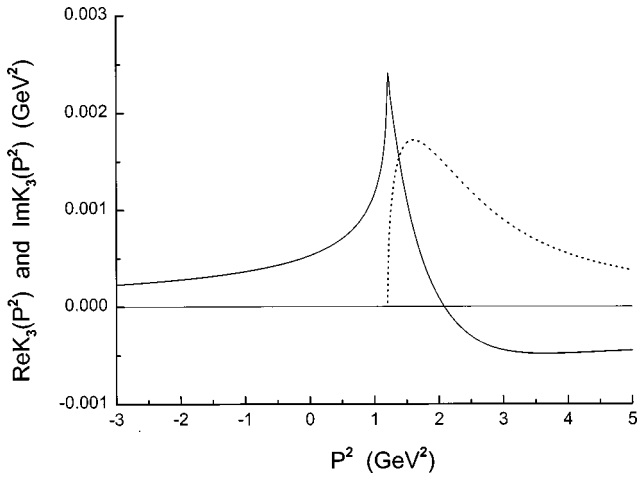

FIG. 10. The values of $\mathrm{Im}\,K_3(P^2)$ and $\mathrm{Re}\,K_3(P^2)$ are shown for the meson channel $\pi\eta'$. Here $\alpha_1=0.325$ GeV.

total width. A peak width of 45 MeV is about one-half the value of about 100 MeV quoted in Refs. [12, 16]. The theoretical analysis of Ref. [18], however, obtains a value of the $m_{a_4}=991$ MeV and a total width of $\Gamma_{a_0}=202$ MeV from the pole position in the complex energy plane. The value of $\Gamma_{\mathrm{peak}}\sim 110$ MeV is given for the peak width, which may be compared to values obtained from Breit-Wigner fits to data: $m_{a_0}=982\pm 3$ MeV, $\Gamma_{\mathrm{peak}}=54\pm 10$ MeV [19] and $m_{a_0}=984\pm 4$ MeV, $\Gamma_{\mathrm{peak}}=95\pm 14$ MeV [20]. Our theoretical analysis yields a peak width of $\Gamma_{\mathrm{peak}}=23$ MeV, which may be adjusted upward by increasing the parameter α_1 or by increasing $\mathrm{Im}\,K_1(P^2)$ (see Fig. 12).

It is occasionally stated that it is natural to assume that the $a_0(1450)$, $K_0^*(1430)$, and $f_0(1370)$ resonances form a nonet based upon a $1\ ^3P_0$ state [21]. However, that observation

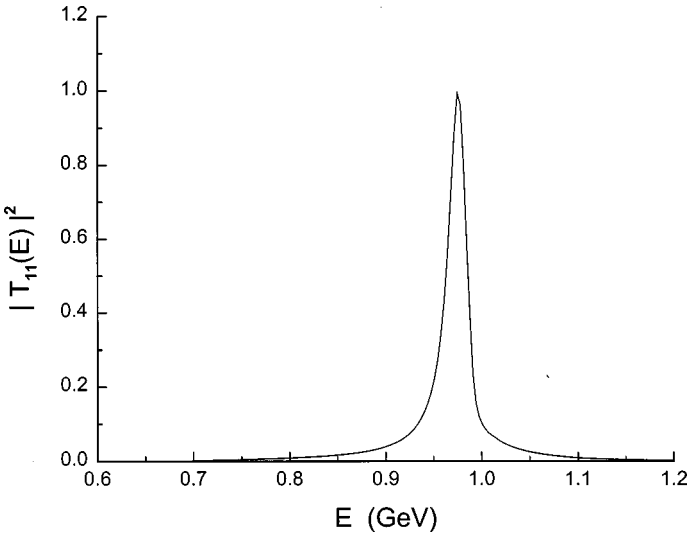

FIG. 11. The solid line represents the values of $|T_{11}(E)|^2$, with $E=\sqrt{P^2}$, obtained when we include the $\pi\ \eta$, $K\bar{K}$, and $\pi\eta'$ decay channels. The width at half maximum is $\Gamma_{\mathrm{peak}}=23$ MeV. Here we use $K_T(P^2)+\Delta K_T$ with $\Delta K_T=0.008$ GeV^2, and $G_{88}=12.46\ \mathrm{GeV}^{-2}$.

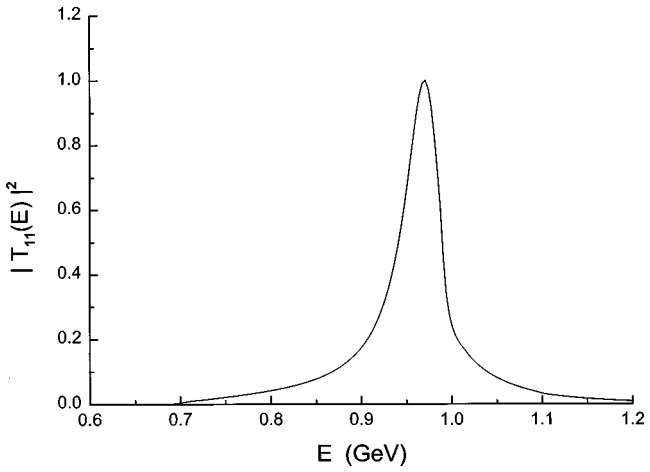

FIG. 12. Here we have replaced $\mathrm{Im}\,K_1(P^2)$ by $2\ \mathrm{Im}\,K_1(P^2)$ and found $\Gamma_{\mathrm{peak}}=47$ MeV. [See caption to Fig. 11.]

requires that the $a_0(980)$ resonance is either a $K\bar{K}$ molecule [22,23] or represents a type of ''threshold effect'' due to the presence of the $K\bar{K}$ threshold at 990 MeV [18]. Those suggestions may be contrasted with the results of our study of a broad range of light mesons and their radial excitations [9]. In our work, the $a_0(980)$ resonance was seen to be a $1\ ^3P_0$ state, while the $a_0(1450)$ resonance appeared as the $2\ ^3P_0$ state. (In Ref. [9] we used a sharp cutoff of $\Lambda_3=0.622$ GeV. The Gaussian parameter $\alpha=0.605$ GeV used here leads to similar results for the spectrum of light mesons.) In Ref. [9], we found the energy of the $T=1$, $1\ ^3P_0$ state to be 1063 MeV, while the $T=1$, $2\ ^3P_0$ state was at 1556 MeV, when we used $G_{88}=12.46\ \mathrm{GeV}^{-2}$ and $\Lambda_3=0.622$ GeV. We have seen that inclusion of $\mathrm{Re}\,K_T(P^2)$ in the formalism moves such states to somewhat lower energy. Thus, from our work, we concluded that the $a_0(980)$ and $K_0^*(1430)$ resonances are in the same nonet, while the $a_0(1450)$ and a (predicted) $K_0^*(1738)$ resonance are in a $2\ ^3P_0$ nonet of states [9]. Our observations are in general accord with those of Törnqvist [12], who describes the $a_0(980)$ resonance as a $T=1q\bar{q}$ state, which is strongly coupled to the $K\bar{K}$ continuum.

While our analysis does not exclude the interpretation of the $a_0(980)$ resonance as a $K\bar{K}$ ''molecule,'' or as a threshold effect, the fact that we find a $J^{PC}=0^{++}$ isovector state at 974 MeV, when we include $\mathrm{Re}\,K_T(P^2)+\Delta K_T$ and use $G_{88}=12.46\ \mathrm{GeV}^{-2}$, is suggestive of a significant $q\bar{q}$ component of the $a_0(980)$. (The use of a sharp cutoff of $\Lambda_3=0.622$ GeV leads to the choice $G_{88}=12.46\ \mathrm{GeV}^{-2}$ made in Ref. [9]. In that case we found $m_{a_0}=1063$ MeV in the absence of $\mathrm{Re}\,K_T(P^2)$, which, if calculated, would lower the value of m_{a_0} somewhat. As noted above, the choice $\alpha=0.605$ GeV yields similar results to those obtained with $\Lambda_3=0.622$ GeV.)

ACKNOWLEDGMENTS

This work was supported in part by a grant from the National Science Foundation and by the PSC-CUNY Faculty Research Award Program.

APPENDIX A

The scalar vertex for our confining interaction was discussed in Ref. [1]. For our model, which has zero energy transfer in the frame with $\mathbf{P}=0$,

$$\overline{\Gamma}_S(P,k)=c_0(P,k)+\hat{\not{k}}c_1(P,k), \tag{A1}$$

with $\hat{k}^\mu=k^\mu-(k\cdot P)P^\mu/P^2$. We define

$$\Lambda^{(+)}(\mathbf{k})\overline{\Gamma}_S(P,k)\Lambda^{(-)}(-\mathbf{k})=\Gamma_S^{+-}(P,k)\Lambda^{(+)}(\mathbf{k})\Lambda^{(-)}(-\mathbf{k}) \tag{A2}$$

and

$$\Lambda^{(-)}(-\mathbf{k})\overline{\Gamma}_S(P,k)\Lambda^{(+)}(\mathbf{k})=\Gamma_S^{-+}(P,k)\Lambda^{(-)}(-\mathbf{k})\Lambda^{(+)}(\mathbf{k}). \tag{A3}$$

The relations between Γ_S^{+-} and Γ_S^{-+} and c_0 and c_1 are

$$\Gamma_S^{+-}(P,k)=c_0(P,k)+mc_1(P,k) \tag{A4}$$

and

$$\Gamma_S^{++}(P,k)=c_0(P,k)-\frac{\mathbf{k}^2}{m}c_1(P,k). \tag{A5}$$

The formalism is made covariant by using Eq. (A1) and the procedure described in Sec. VI of Ref. [1].

Equations for Γ_S^{+-} and Γ_S^{-+} were given in Ref. [1]. We repeat those equations here, taking the opportunity to correct two misprinted signs. With $k=|\mathbf{k}|$ and $k'=|\mathbf{k}'|$, we have

$$\Gamma_S^{+-}(P^0,|\mathbf{k}|)=1-4\pi\int\frac{k'^2dk'}{(2\pi)^3}\left[\frac{-8k'^2}{E(\mathbf{k}')}\right]\times\frac{V_0^C(k,k')+(m^2/2kk')V_1^C(k,k')}{(P^0)^2-[2E(\mathbf{k}')]^2}\times\Gamma_S^{+-}(P^0,k') \tag{A6}$$

and

$$\Gamma_S^{++}(P^0,|\mathbf{k}|)=1-4\pi\int\frac{k'^2dk'}{(2\pi)^3}\left[\frac{-8k'^2}{E(\mathbf{k}')}\right]\times\frac{V_0^C(k,k')-(k/2k')V_1^C(k,k')}{(P^0)^2-[2E(\mathbf{k}')]^2}\Gamma_S^{+-}(P^0,k'). \tag{A7}$$

In these equations

$$V_l^C(k,k')=\frac{1}{2}\int_{-1}^{1}dxP_l(x)V^C(\mathbf{k}-\mathbf{k}'). \tag{A8}$$

Coupled equations for $c_0(P,k)$ and $c_1(P,k)$ are

$$c_0(P,k)=1-4\pi\int\frac{k'^2dk'}{(2\pi)^3}\left[\frac{-8k'^2}{E(\mathbf{k}')}\right]\times\frac{V_0^C(k,k')[c_0(P,k')+mc_1(P,k')]}{(P^0)^2-[2E(\mathbf{k}')]^2} \tag{A9}$$

and

$$c_1(P,k)=4\pi\int\frac{k'^2dk'}{(2\pi)^3}\left[\frac{4mk'/k}{E(k')}\right]\times\frac{V_1^C(k,k')[c_0(P,k')+mc_1(P,k')]}{(P^0)^2-[2E(\mathbf{k}')]^2}, \tag{A10}$$

where we have again corrected two misprinted signs that appear in Ref. [1]. Note that $\Gamma_S^{+-}(P^0,|\mathbf{k}|)$ is singular when the homogeneous version of Eq. (A6) has a solution. At those points, the eigenvalue P^0 is the energy of one of the bound states in the confining field (see Fig. 4).

We remark that, except for small values of P^0, we usually make the replacement

$$\frac{1}{(P^0)^2-[2E(\mathbf{k})]^2}\rightarrow\frac{1}{4E(\mathbf{k})}\frac{1}{P^0-2E(\mathbf{k})} \tag{A11}$$

in Eqs. (A6)–(A10).

APPENDIX B

In this appendix we describe our treatment of the η and η'. For these mesons we included the full vertex structure, as well as our model of confinement. In Refs. [6] and [9], we calculated the η and η' vertices, which took the form

$$V_\eta(P)=g_{\eta qq}i\gamma_5[-\sin\hat{\theta}\lambda_0+\cos\hat{\theta}\lambda_8]+\frac{\tilde{g}_{\eta qq}}{2}i\not{P}\gamma_5[-\sin\tilde{\theta}\lambda_0+\cos\tilde{\theta}\lambda_8], \tag{B1}$$

where $\not{P}$ is the η (or η') momentum *entering* the vertex. Inclusion of confinement led to the form [6,8]

$$\tilde{V}_\eta(P,k)=g_{\eta qq}i\gamma_5[b_0(P,k)+\not{P}b_1(P,k)][-\sin\hat{\theta}\lambda_0+\cos\hat{\theta}\lambda_8]+\frac{\tilde{g}_{\eta qq}}{2m_{us}}i\not{P}\gamma_5[d_0(P,k)+\not{P}d_1(P,k)]\times[-\sin\tilde{\theta}\lambda_0+\cos\tilde{\theta}\lambda_8]. \tag{B2}$$

For the purpose of this work, we have introduced the constants

$$h_1=g_{\eta qq}\,\mathrm{Tr}[-\sin\hat{\theta}(\lambda_3^2\lambda_0)+\cos\hat{\theta}(\lambda_3^2\lambda_8)], \tag{B3}$$

and

$$h_2=\frac{\tilde{g}_{\eta qq}}{2m_{us}}\mathrm{Tr}[-\sin\tilde{\theta}(\lambda_3^2\lambda_0)+\cos\tilde{\theta}(\lambda_3^2\lambda_8)]. \tag{B4}$$

In Ref. [8] we have found the parameters for the η to be $g_{\eta qq}=5.97$, $\tilde{g}_{\eta qq}=1.45$, $\hat{\theta}=-11.2°$, $\tilde{\theta}=-15.1°$, when we put $m_{us}=0.433$ GeV and used a Gaussian cutoff with $\alpha=0.605$ GeV. For the η', the parameters were $g_{\eta' qq}=4.66$, $\tilde{g}_{\eta' qq}=1.58$, $\hat{\theta}=-115.5°$, and $\tilde{\theta}=-107.5°$ for the same Gaussian cutoff. Equation (B2) may be rewritten as a term proportional to $i\gamma_5$ and another term proportional to $i\not{P}\gamma_5$. The term proportional to $\not{P}$ gave rise to the contributions $M_1^{\eta'\pi(2)}(P^2)$ and $M_2^{\eta'\pi(2)}(P^2)$, introduced in Eqs. (3.2) and (3.5). These terms are rather lengthy, so we do not reproduce them here. Various figures in Ref. [8] exhibit the functions b_0, b_1, d_0, and d_1 for $P^2=m_\eta^2$ and $P^2=m_{\eta'}^2$, with $m_\eta=547$ MeV and $m_{\eta'}=958$ MeV.

APPENDIX C

In this appendix we describe our treatment of the pion and kaon vertex functions. If P is the momentum entering the vertex, the vertex for the pion is

$$i\bar{\Gamma}_5(P)=i\gamma_5\left[\cos\theta_P-\frac{\not{P}}{\sqrt{P^2}}\sin\theta_P\right]. \tag{C1}$$

We found $\theta_P=-3.09°$ and $g_{\pi qq}=4.57$. For the kaon, we have $g_{Kqq}=8.09$ and

$$i\bar{\Gamma}_K(P,k_c)=i\left\{\gamma_5\cos\theta_K[b_0+b_1\not{P}+b_2\hat{\not{k}}_c]+\sin\theta_K\frac{\not{P}\gamma_5}{\sqrt{P^2}}[d_0+\not{P}d_1]\right\}, \tag{C2}$$

with $\theta_K=-7.05°$. The various functions, $b_0=b_0(\sqrt{P^2},\sqrt{-k_c^2})$, etc., that implement our model of confinement are described in Ref. [14], where figures representing these functions are presented. [In the case that P is the momentum leaving the vertex, we need to change the sign of $\not{P}$ and $\hat{\not{k}}_c$ in Eq. (C2).]

For simplicity, in this work we use $i\bar{\Gamma}_5(P)=i\gamma_5$, with $g_{\pi qq}=3.93$ and $i\bar{\Gamma}_K(P,k_c)=i\gamma_5$ with $g_{Kqq}=8.09$. However, we include the full complexity of the η and η' vertices as described in Appendix B.

[1] L. S. Celenza, Xiang-Dong Li, and C. M. Shakin, Phys. Rev. C **55**, 3083 (1997).

[2] L. S. Celenza, Xiang-Dong Li, and C. M. Shakin, Phys. Rev. C **56**, 3326 (1997).

[3] Bo Huang, Xiang-Dong Li, and C. M. Shakin, Phys. Rev. C **58**, 3648 (1998).

[4] L. S. Celenza, Bo Huang, and C. M. Shakin, Phys. Rev. C **58**, 1845 (1998).

[5] L. S. Celenza, Bo Huang, and C. M. Shakin, Phys. Rev. C **59**, 1041 (1999).

[6] L. S. Celenza, Bo Huang, and C. M. Shakin, Phys. Rev. C **59**, 1030 (1999).

[7] L. S. Celenza, Bo Huang, and C. M. Shakin, Phys. Rev. C **59**, 1700 (1999).

[8] L. S. Celenza, Bo Huang, and C. M. Shakin, Phys. Rev. C **59**, 2814 (1999).

[9] L. S. Celenza, Bo Huang, Huangsheng Wang, and C. M. Shakin, Phys. Rev. C **60**, 025202 (1999).

[10] L. S. Celenza, Bo Huang, Huangsheng Wang, and C. M. Shakin, Phys. Rev. C **60**, 035206 (1999).

[11] L. S. Celenza, Bo Huang, Huangsheng Wang, and C. M. Shakin, Brooklyn College Report BCCNT 99/031/279, 1999 (unpublished).

[12] N. A. Törnqvist, Z. Phys. C **68**, 647 (1995).

[13] L. S. Celenza, Shun-fu Gao, Bo Huang, Huangsheng Wang, and C. M. Shakin, Brooklyn College Report BCCNT 99/111/282, 1999, Phys. Rev. C (submitted).

[14] L. S. Celenza, Bo Huang, Huangsheng Wang, and C. M. Shakin, preceding paper, Phys. Rev. C **60**, 065209 (1999).

[15] Particle Data Group, C. Caso, *et al.*, Eur. Phys. J. C **3**, 1 (1998).

[16] N. A. Törnqvist and M. Roos, Phys. Rev. Lett. **76**, 1575 (1996).

[17] A. Abele, *et al.* Phys. Rev. D **57**, 3860 (1998).

[18] G. Janssen, B. C. Pearce, K. Holinde, and J. Speth, Phys. Rev. D **52**, 2690 (1995).

[19] A. Amlser *et al.*, Phys. Lett. B **291**, 347 (1992).

[20] A. Armstrong *et al.*, Z. Phys. C **52**, 389 (1991).

[21] D. V. Bugg, V. V. Anisovich, A. Sarantsev, and B. S. Zou, Phys. Rev. D **50**, 4412 (1994).

[22] N. N. Achasov and V. V. Gubin, Phys. Rev. D **56**, 4084 (1997).

[23] N. N. Achasov, V. V. Gubin, and V. I. Shevchenko, Phys. Rev. D **56**, 203 (1997).